PROCEEDINGS OF SPIE

SPIEDigitalLibrary.org/conference-proceedings-of-spie

Investigating the contributions of anatomical variations and quantum noise to image texture in digital breast tomosynthesis

William H. Nisbett, Amar Kavuri, Mini Das

William H. Nisbett, Amar Kavuri, Mini Das, "Investigating the contributions of anatomical variations and quantum noise to image texture in digital breast tomosynthesis," Proc. SPIE 10573, Medical Imaging 2018: Physics of Medical Imaging, 105730H (9 March 2018); doi: 10.1117/12.2294981

SPIE.

Event: SPIE Medical Imaging, 2018, Houston, Texas, United States

Investigating the contributions of anatomical variations and quantum noise to image texture in digital breast tomosynthesis

William H. Nisbett[a], Amar Kavuri[b], and Mini Das[a,b,*]

[a]University of Houston Department of Physics
[b]University of Houston Department of Biomedical Engineering
[*]Email: mdas@uh.edu

ABSTRACT

Our previous work on DBT image texture indicates that certain texture features may impact human observer performance for the task of low-contrast mass detection. Despite this, little is yet known about these texture statistics in the context of medical imaging. In this study, we investigate the factors that influence texture features in simulated DBT images. Specifically, we explore whether or not changes in quantum noise and anatomical variations are reflected in image texture curves. Our findings concerning the effects of Wiener filtration and changes in DBT system parameters indicate that texture statistics are affected by both anatomical variations and quantum noise.

1. INTRODUCTION

Optimization of imaging systems with radiological tasks in mind is critical to improving the diagnostic power of a modality. The task of optimizing acquisition geometry is especially relevant to Digital Breast Tomosynthesis (DBT), where there are several key parameters that can be changed. In order to evaluate different acquisition geometries, Receiver Operator Characteristic (ROC) analysis and its derivatives (e.g. LROC) are typically employed.[1,2] Within the realm of assessing imaging systems through observer performance, human observers still remain as the gold standard. However, conducting human observer ROC studies is both time and resource intensive, thus creating the opportunity for a cheaper alternative to flourish.

Texture features are a class of computationally inexpensive metrics that characterize image appearance. Amongst these, several texture statistics belong to a subcategory known as second-order texture features, which utilize pixel-by-pixel gray-level relationships in order to describe image texture.[3] Previously, some groups have explored the possibilities of using image texture for risk assessment in medical images.[4–6] Findings from our previous work on image texture show that texture features vary significantly with DBT system parameters and that certain second-order texture features correlate well with human observer performance for the task of low-contrast mass detection.[7] In spite of this, fundamental aspects of medical image texture still remain unclear. In this study, we investigate the physical origins of texture through examining the contributions of quantum noise and anatomical variations to six texture features identified in our previous study as having strong correlations with human observer performance.

2. METHODOLOGY

2.1 Breast and Mass Models

The breast phantoms used in this study are anthropomorphic software breast volumes generated by Bakic et al. at the University of Pennsylvania.[8] Each phantom was simulated with one of three different volumetric glandular fractions (VGF), 25%, 50%, or 75%, so as to mimic breasts of different densities. To create the set of lesion-present cases utilized in our LROC study, a single homogeneous, spherical lesion of 8-mm diameter was inserted at a random position within the fibroglandular compartment of a subset of the phantoms. The attenuating properties of these lesions modeled those of infiltrating ductal carcinoma as a function of energy and were based upon empirical measurements.

Medical Imaging 2018: Physics of Medical Imaging, edited by Joseph Y. Lo, Taly Gilat Schmidt, Guang-Hong Chen, Proc. of SPIE Vol. 10573, 105730H
 · doi: 10.1117/12.2294981

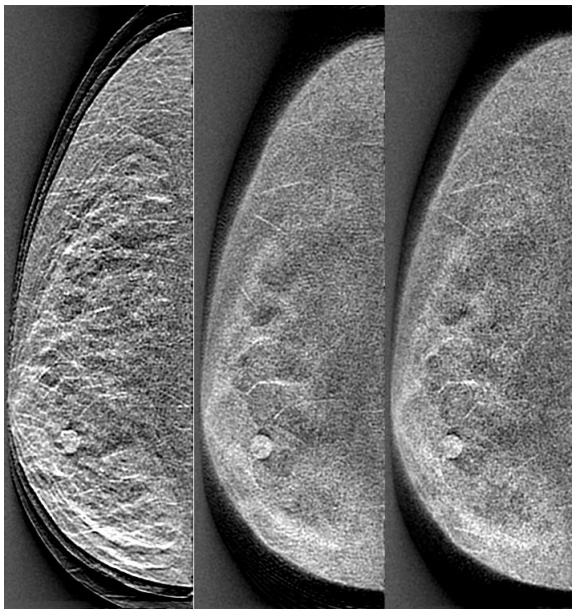

Figure 1: An example of three simulated DBT images used in our study. Each image is of the same 25% dense phantom taken over a 60^o span with varying numbers of projections (from left to right: 3, 19, and 41). A target lesion is present in the bottom-left region of each image.

2.2 Image Generation

DBT imaging data was created using a rigorous computer simulation, which accounted for both focal-spot blur and scintillator blur.[9] In the simulation, Siddons ray-tracing method was utilized to model x-ray transmission through the phantom.[10] A serially cascaded linear systems model was implemented to model signal and noise propagation through a CSI-based amorphous silicon at-panel detector. Quantum detector efficiency, scintillator gain, and optical collection efficiency were also considered in this step. In each simulation, a number of projections, P, was acquired through some angular span, β, of the phantom, where $P \in \{3, 7, 11, 15, 19, 21, 25, 31, 35, 41, 45, 51\}$ and $\beta = 60^o$. For each simulation, a total amount of Poisson noise equivalent to 1.5 mGy of dose was evenly distributed across the P projections.

Reconstruction was performed using Feldkamps filtered back projection (FBP) method, which was then followed by the application of a 3D Butterworth filter (0.25 cycles/pixel cut-off frequency). From each reconstructed volume of data, a single slabbed image of 1mm thickness was produced. For lesion-present cases, this was achieved by first locating the slice that intersected the lesion's center, and then performing a boxcar average of this slice with the two slices above and two slices below it. In the case of lesion-free phantoms, a random slice in the volume was chosen and the same slabbing procedure was performed to produce the final image. Examples of the simulated images can be seen in Fig. 1. A total of 1728 images were simulated with each of the three phantom densities comprising exactly one-third of the total images.

2.3 LROC Study

Two non-radiologists participated in the human LROC study, reading images obtained with an angular span of 60^o for a subset of the projection numbers (3, 7, 25, 45). In this study, observers were tasked with determining whether or not a lesion was present in each image, as well as assigning a confidence rating to their decision. In addition, when categorizing an image as lesion-present, observers were also tasked with localizing the lesion to within a 15-by-15 square-pixel region of its center. For each projection number in the aforementioned subset, participants read a 25% and 50% combined-density set of 144 images. Wilcoxon estimates of the Area Under the LROC Curve (AUC) were utilized to assess observer performance. For each set of images, observer performance was then averaged across all observers.

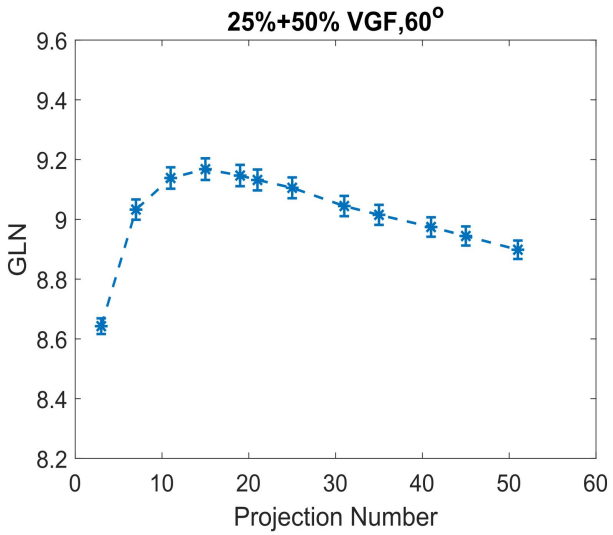

Figure 2: Texture features, such as GLN, vary as a function of projection number and also correlate strongly with observer performance.

2.4 Texture Analysis

Analysis of DBT image texture was performed using MATLAB (R2016a). Prior to ROI selection and texture analysis, image pixels were linearly quantized from intensity values into 256 gray-levels. Black and white thresholds (i.e. thresholds for bins 0 and 255 respectively) for each image were automatically determined at runtime and were chosen in such a way as to eliminate the influence of the background on pixel quantization. A 9-by-4 lattice of ROIs covering a total area of 315-by-140 square-pixels was created atop the central, dense region of the breast since, clinically, breast abnormalities are more frequent in this area. Texture analysis was performed separately on each of these ROIs through the calculation of six texture descriptors, each of which was derived from one of three spatial gray-level matrices: the Gray-level Co-occurrence Matrix (GLCM),[11] the Neighborhood Gray-tone Difference Matrix (NGTDM),[12] and the Run Length Matrix (RLM).[13] Definitions for all texture features were taken from the literature and are explicitly given in Table 1. The texture features in a given image were averaged across all ROIs and then these average textures feature for each image in a set were then averaged once more across the entire set.

Type	Feature	Definition
GLCM	Homogeneity	$\sum_{i,j} \frac{G(i,j)}{1+\lvert i-j\rvert}$
	Entropy	$-\sum_{i,j} G(i,j) log_2(G(i,j))$
	Energy	$\sum_{i,j} G(i,j)^2$
NGTDM	Contrast	$[\frac{1}{N_g(N_g-1)} \sum_{i,j} P_i P_j (i-j)^2][\frac{1}{n^2} \sum_i D(i)]$
	Complexity	$\sum_{i,j} \{\lvert i-j\rvert / (n^2 P_i + n^2 P_j)\}\{P_i D(i) + P_j D(j)\}$
RLM	Gray Level Nonuniformity	$\frac{1}{N} \sum_i (\sum_j R(i,j))^2$

Table 1: Definitions for each of the six statistics utilized in this study.

3. RESULTS & DISCUSSION

In the case of each texture feature, a gradual change in feature magnitude is noted at relatively large projection numbers. Specifically, for positively correlating statistics this change is a decrease, while for negatively correlating statistics it is an increase. Visual inspection of the images reveals that image quality appears to slightly worsen

at large projection numbers due to a subtle increase in image noise. In DBT, it is well known that as the number of projections is increased and total dose is kept constant, the noise content per slice increases as well. One would expect this increasing quantum noise to hinder observer performance at higher projections, which is indeed the case according to our previous work.[7]

Figure 3: A side-by-side comparison of a lesion-present image before (left) and after (right) application of an adaptive Wiener filter.

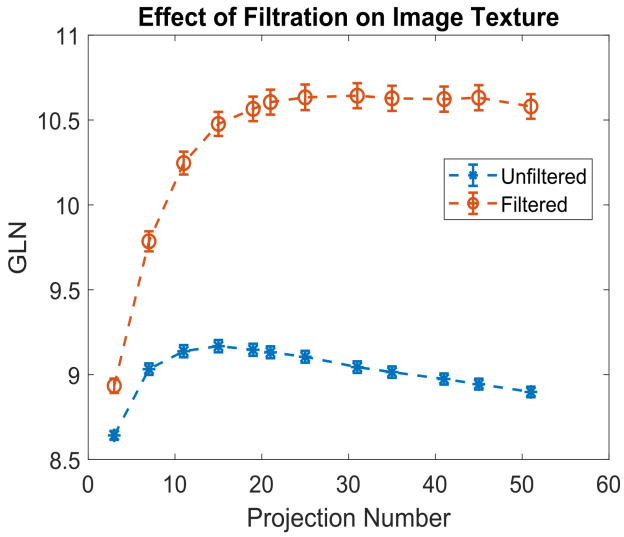

Figure 4: Comparison of GLN texture curves for filtered and unfiltered images.

To confirm this, an adaptive Wiener filter[14] was applied to the projections prior to reconstruction and slabbing. A visual comparison of these Wiener-filtered DBT images with those unfiltered ones reveals that the image quality drastically improved due to application of the filter (Fig. 3). Texture analysis of these newly filtered images elicits interesting findings, especially when compared with the unfiltered texture. The texture curve for

each feature experienced a significant change at high projection numbers; rather than changing gradually as projection number increases, the texture becomes nearly constant at high projections (Fig. 4). Furthermore, an overall increase in positively correlating feature values (and decrease in negatively correlating feature values) was noted at all projections. In terms of observer performance, this implies that application of the Wiener filter should improve observer performance at all projection numbers, which one would expect. In sum, these results indicate that texture is significantly affected by quantum noise and that a causal relationship between image texture and observer performance still remains plausible.

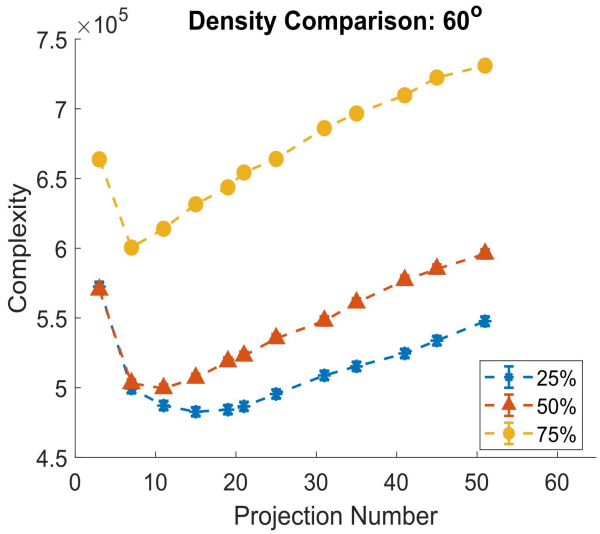

Figure 5: A comparison of Complexity in image sets with different densities reveals that texture features are affected by breast density.

In order to determine whether or not anatomical variations impact image texture, texture curves for all three densities of phantom were compared (Fig. 5). Increases in breast density saw feature magnitudes decrease in positively correlated statistics and increase in negatively correlated statistics. In terms of observer performance, this indicates that higher breast density hinders an observer's ability to detect low-contrast masses, which is again in line with our expectations. Furthermore, this result also indicates that texture features are indeed impacted by anatomical variations and the amount of structural information available in an image. Finally, there appears to be a negative relation between breast density and the peak number of projections; that is, as breast density increases, the peak number of projection decreases for both positively and negatively correlated features alike.

4. CONCLUSIONS AND FUTURE WORKS

Based on our results, it is clear that not only do DBT system parameters such as acquisition span and projection affect image texture, but reconstruction methods such as filtering do as well. As such, using image texture to draw conclusions about the content of medical images should be avoided since it is heavily impacted by system parameters and reconstruction methods. In this study, we also showed that both quantum and anatomical noise individually contribute to image texture and also found that trends observed in the texture features continued to match with expectations and previous research concerning observer performance for the task of low-contrast mass detection. As a result, these findings both shed light on the fundamental processes that influence image texture and also further support the idea that image texture may indeed impact observer performance. In the future, we intend to expand the set of texture features in our analysis to include not only those of the secondary variety, but also higher order features as well. Future works could also include investigating the effects of varying filter strength on image texture and also examining the spatial distribution of feature magnitudes in images.

Acknowledgments

This work was partially supported by funding from the US Department of Defense (DOD) Congressionally Directed Medical Research Program (CDMRP) Breakthrough Award BC151607 and the National Science Foundation CAREER Award 1652892. We would also like to thank Dr. Predrag Bakic from the University of Pennsylvania for supplying the phantoms utilized in this study.

REFERENCES

1. Zweig, M. H. and Campbell, G., "Receiver-operating characteristic (ROC) plots: A fundamental evaluation tool in clinical medicine," *Clinical Chemistry* **39**(4), 561–577 (1993).
2. Fawcett, T., "An introduction to ROC analysis," *Pattern Recognition Letters* **27**(8), 861–874 (2006).
3. Materka, A. and Strzelecki, M., "Texture Analysis Methods A Review," *Methods* **11**, 1–33 (1998).
4. Kontos, D., Ph, D., Bakic, P. R., and Carton, A.-k., "Parenchymal Texture Analysis in Digital Breast Tomosynthesis for Breast Cancer Risk Estimation: A Preliminary Study," *Academic radiology* **16**(3), 283–298 (2009).
5. Zheng, Y., Keller, B. M., Ray, S., Wang, Y., Conant, E. F., Gee, J. C., and Kontos, D., "Parenchymal texture analysis in digital mammography: A fully automated pipeline for breast cancer risk assessment," *Medical Physics* **42**(7) (2015).
6. Gastounioti, A., Conant, E. F., and Kontos, D., "Beyond breast density: A review on the advancing role of parenchymal texture analysis in breast cancer risk assessment," *Breast Cancer Research* **18**(1), 1–12 (2016).
7. Nisbett, W. H., Kavuri, A., Fredette, N. R., and Das, M., "On the impact of local image texture parameters on search and localization in digital breast imaging," *Proceedings of SPIE* **10136**(March 2017), 1–6 (2017).
8. Bakic, P. R., Zhang, C., and Maidment, A. D., "Development and characterization of an anthropomorphic breast software phantom based upon region-growing algorithm," *Medical Physics* **38**(6), 3165–3176 (2011).
9. Vedula, a. a., Glick, S. J., and Gong, X., "Computer simulation of {CT} mammography using a flat-panel imager," *Proc. SPIE 5030 Medical Imaging 2003: Phys. Med. Im.* **5030**, 349–360 (2003).
10. Siddon, R. L., "Fast calculation of the exact radiological path for a three-dimensional ct array," *Medical Physics* **12**(2), 252–255 (1985).
11. Haralick, R. M., Shanmugam, K., and Dinstein, I., "Textural Features for Image Classification," *IEEE Transactions on Systems, Man, and Cybernetics* **SMC-3**(6), 610–621 (1973).
12. Amadasun, M. and King, R., "Texural Features Corresponding to Texural Properties," *IEEE Transactions on Systems, Man and Cybernetics* **19**(5), 1264–1274 (1989).
13. Galloway, M. M., "Texture analysis using gray level run lengths," *Computer Graphics and Image Processing* **4**(2), 172–179 (1975).
14. Marcelo A. C. Vieira, Predrag R. Bakic, A. D. A. M., "Effect of denoising on the quality of reconstructed images in digital breast tomosynthesis," *Proc.SPIE* **8668**, 8668 – 8668 – 14 (2013).